Progress In Electromagnetics Research M, Vol. 58, 73–86, 2017

Modelling Dispersive Behavior of Excitable Cells

Soheil Hashemi[1, 2] and Ali Abdolali[1, 2, *]

Abstract—Most of the materials have nearly constant electromagnetic characteristics at low frequencies. Nonetheless, biological tissues are not the same; they are highly dispersive, even at low frequencies. Cable theory is the most famous method for analyzing nerves though a common mistake when studying the model is to consider a constant parameter versus frequency. This issue is discussed in the present article, and the analysis of how to model the dispersion in the cable model is proposed and explained. The proposed dispersive model can predict the behavior of excitable cells versus stimulations with single frequency or wide-band signals. In this article, the nondestructive external stimulation by a coil is modeled and computed by finite difference method to survey the dispersion impact. Also, 5% to 80% difference is shown between the results of dispersive and nondispersive models in the 5 Hz to 4 kHz investigation. The disagreement expresses the dispersion notability. The proposed dispersive method assists in accurate device design and signal form optimization. Noise analysis is also achieved by this model, unlike the conventional models, which is essential in the analysis of single neurons or central nervous system, EEG and MEG records.

1. INTRODUCTION

In many studies, the behavior of excitable cells is predicted by simulation. Cable equations are proposed to simulate the activity of nerves [1–3]. External electrical stimulation was studied only by experiments before Roth and Basser proposed an equation that included induced electrical field (E-field). This equation is used to predict the effects of stimulator parameters on the activities of nerve cells [4].

Optimization in pulse width and energy of stimulators is also noteworthy in this area. Since these criteria depend on the geometry of stimulators, most researchers do not introduce the best stimulator, but the results can be helpful in future designs [5–9]. Obtaining the thresholds of excitability, which depends on the stimulator parameters, is common in the literature [4, 10–15]. In all of these pieces of research, diagrams such as excitability thresholds and parameter impact are determined to help the design of stimulators and cognition of excitable cells. Howell et al. investigated the effects of dispersive capacitance by a simple model and the significance of dispersion though a more accurate model was required for expressing the cell behavior [16]. Results of all the mentioned works may vary after considering the dispersion diagram of materials according to the chosen frequency of analysis.

The interaction of electromagnetic radiation with biological tissues at cellular and molecular levels eventuates dielectric properties. The mechanisms of the interaction are discussed in the literature. Biological tissues are highly dispersive and vary versus frequency, even at extremely low frequencies [17]. Both conductivity and permittivity are dispersive in biological tissues. These parameters are equivalent to resistance and capacitance, respectively, in the cable model of excitable cells. The features of the dielectric of a biological tissue are briefly reported below.

Dispersion, in the gigahertz region, is associated with the polarization of water molecules. In the hundreds of kilohertz region, dispersion is due to the polarization of cellular membranes. The membranes

Received 1 March 2017, Accepted 2 June 2017, Scheduled 4 July 2017

* Corresponding author: Ali Abdolali (abdolali@iust.ac.ir).

[1] Department of Electrical Engineering, Iran University of Science and Technology (IUST), Narmak, Tehran, Iran. [2] Bioelectromagnetics Lab, Iran University of Science and Technology, Iran.

act as barriers to the flow of ions between the extra and intracellular media. The dispersion in the low frequency region is due to ionic diffusion processes at the site of the cellular membrane. The membrane admittance is measured between 100 Hz and 100 kHz, and the dielectric properties of the membrane of neural cells differ from other biological properties [18–22].

Howell et al. investigated the effect of dispersive capacitance, but their proposed model did not consider an anomalous inductive reactance behavior [16]. The Howell model considers only the effect of dispersive capacitance and neglects the dispersive conductance. Our model considers both the anomalous inductive reactance behavior and dispersive conductance in addition to dispersive capacitance. The velocity of the movement of ions, due to the electrical field per frequency, defines the conductance of the ionic materials. This velocity differs by the frequency of the induced E field, and consequently, the conductance differs by frequency. This issue results in dispersion diagrams for conductance, as mentioned before. Conductance influences both potential propagation speed and distribution.

In Figure 1, the capacitance of motor neuron versus frequency is shown [18–22]. This figure illustrates the concept of dispersion. Therefore, although some assumptions of the quasi-static analysis are applied, it is necessary to consider the effect of dispersion in the analysis.

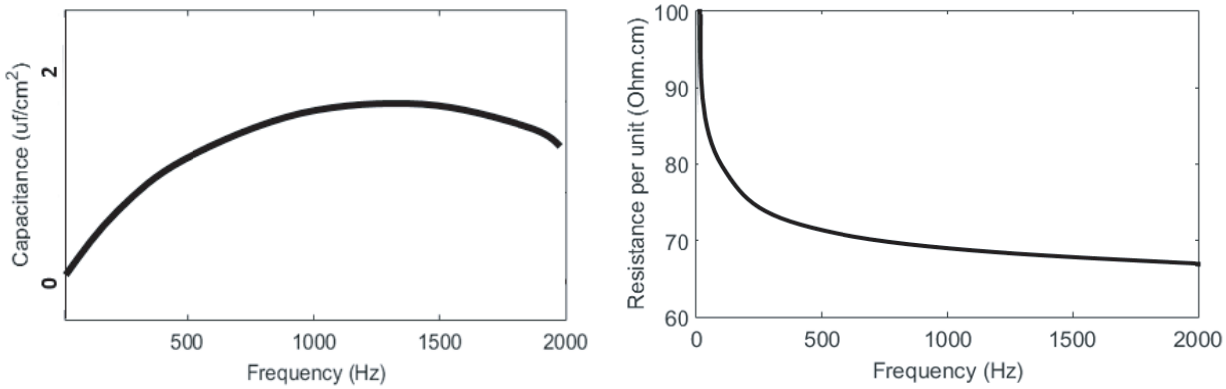

Figure 1. Resistance and capacitance diagram of a neuron fiber is retrieved and sketched versus frequency based on the references. Variations in both characteristics are considerable [18–22].

The measured capacitance is strongly dependent upon frequency. Below 300 Hz, the capacitance decreases markedly; on the other hand, conductance begins to increase as the frequency further decreases. This behavior is called an anomalous inductive reactance [18, 20–24]. Above 300 Hz, the measured capacitance decreases with the increasing frequency, and conductance increases at the same time as most biological tissues. Measurements of tissue dielectrics at different frequencies are made and parametric Cole-Cole models are fitted to these measurements [17, 20–25]. However, since Cole-Cole models cannot be easily expressed in the time domain, Debye and Lorentz models are often used instead in the simulations.

Most research has declared longitudinal external field as the effective field [26–29]. Other work has been focused on the analysis of rotationally asymmetric potential, although this scenario is reported to be less effective than the longitudinal electric field in experiments [30]. Below, we propose and discuss the basis of the dispersive method. Although it is capable of considering both transverse and longitudinal external electric fields, we only consider the longitudinal mode to explain the idea clearly. The finite difference method is chosen in this work due to the demands. Nondispersive and dispersive models are compared, and the results are shown and studied in the results and discussion sections.

2. METHOD AND ANALYSIS

Although modeling the effects of electric (E) field on the nerve fibers has been discussed since 1990, dispersion has not been considered in the literature. Consider the modified Hodgkin-Huxley model

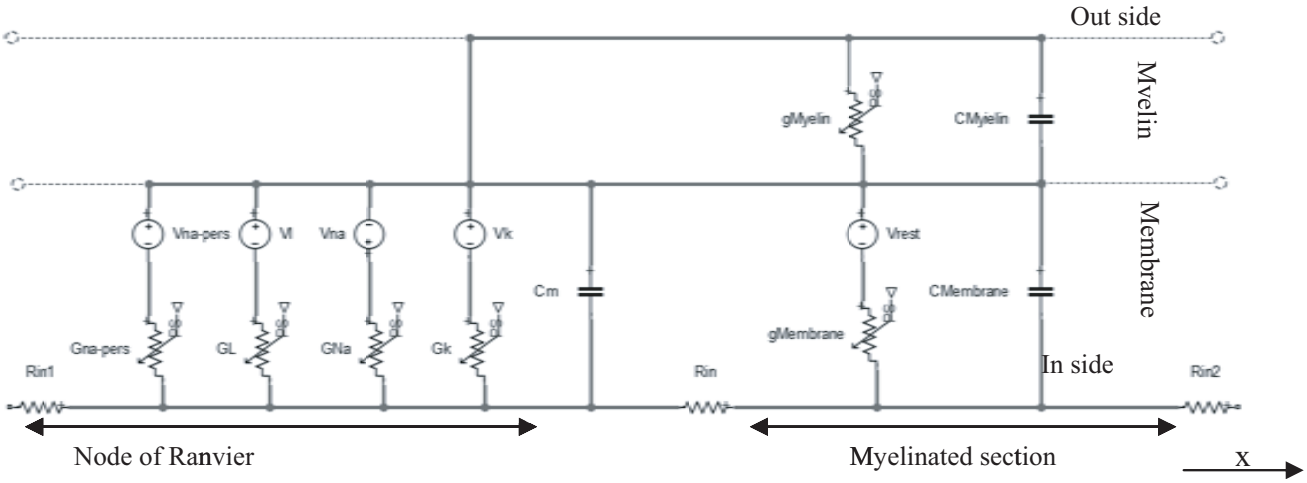

Figure 2. Circuit model of modified cable model by McIntyre including myelinated and Ranvier sections. Length of myelinated segments is 1.5 mm. The nodal membrane dynamics include fast (GNa) and persistent (Gna-pers) sodium, slow potassium (GK) and linear leakage (GL) conductance in parallel with the nodal capacitance (Cm) [31, 32].

by McIntyre in Figure 2 [31, 32]. The capacitance and resistance are the dispersive parameters. This model is expressed by Equations (1) and (2). Equation (1) describes Ranvier nodes, and Equation (2) describes myelin nodes.

$$r_0/2\rho \frac{\partial^2 V_m}{\partial x^2} - C\frac{\partial V_m}{\partial t} - \sum g_{(V_m)k}(V_m - V_{I-ch.k}) = 0 \tag{1}$$

$$r_0/2\rho_{myelin} \frac{\partial^2 V_m}{\partial x^2} - C_{myelin}\frac{\partial V_m}{\partial t} = 0 \tag{2}$$

where V_m is the membrane potential at each node, V_{i-chk} the kth source voltage for each of the kth ion channel, g_k the voltage-dependent conductivity due to the kth ion channels, r_0 the radius of the nerve fiber, and ρ the intracellular resistance per unit. These equations are valid for each node of the fibers and the parameters may be different at each node.

Two terms of $1/\rho\frac{\partial^2 V_m}{\partial x^2}$ and $C\frac{\partial V_m}{\partial t}$ in Equations (1) and (2) demonstrate the effect of capacitance and resistance, respectively. These parameters are equivalent to the permittivity and conductivity of the tissues. The diagrams in Figure 1 show highly variable capacitance and resistance versus frequency; thus, a constant value is inaccurate. Magnitude of C is important in $C\partial V_m/\partial t$ to specify how the membrane potential changes. Besides, consider the transformation of a single action potential signal into frequency domain by Fourier transform. By eliminating the constant component of a single action potential and transform, the Fourier transform of the signal is shown in Figure 3. Considering the spectrum in Figure 3 and voluntary excitation signal at any frequency, the constant C may not be appropriate for both action potential and excitation signal.

First, we discuss how to model the dispersion diagram; then, we propose how to use it in the cable equation. Debye and Lorentz models are the most famous models used to show dispersion versus frequency. The Debye dispersion is characterized as a function of frequency by the following expression for relative permittivity [17]:

$$\varepsilon_{(\omega)} = \varepsilon_\infty + \sum_i^N \frac{\varepsilon_0 \Delta\varepsilon_{r_i}}{1 + j\omega\tau_{p_i}} \tag{3}$$

where τ_{p_i} is the relaxation time of the ith Debye pole, $\Delta\varepsilon_{r_i}$ the corresponding relative permittivity increment, ε the complex permittivity, and ω the angular frequency. Each $\varepsilon_0\Delta\varepsilon_{r_i}/(1 + j\omega\tau_{p_i})$ is valid for a limited frequency band and the sum of these terms results the total dispersion diagram. The

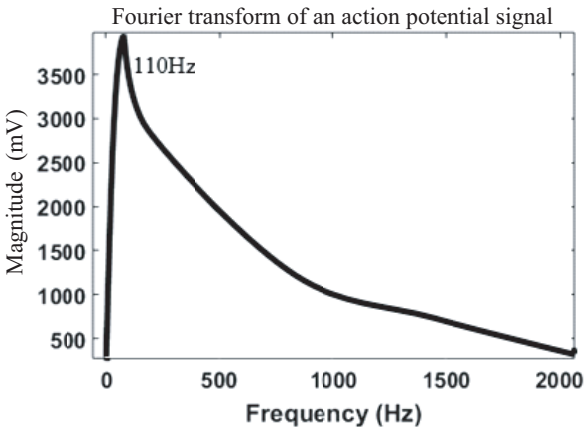

Figure 3. Fourier transform of a single action potential signal. The constant component of the signal is eliminated before transform. The characteristics of the fiber are mentioned in Table 2.

defining expression for the Lorentz dispersion is [33]:

$$\varepsilon_{(\omega)} = \varepsilon_\infty + \sum_i^N \frac{j\omega\varepsilon_0\varepsilon_{a_i}}{1 + j\omega\tau_{a_i} - \omega^2/\omega_{a_i}^2} \tag{4}$$

where ω_{a_i} is the undamped resonant frequency of the ith Lorentz pole-pair, τ_{a_i} the corresponding damping factor, N the required number of terms, ε_0 the permittivity of free space, and ε_{a_i} the corresponding relative permittivity increment. Each denominator has two complex roots. Different materials may have different dispersion relations and can be fitted by the models in Equations (3) and (4).

The dispersion relations show the electromagnetic properties of materials according to the properties at the past time and present potential. The ionic conductance is time- and potential-dependent. These relations are derived from measurements in a variety of situations in time and show the conductance at the present time. Dispersion and nonlinearity are already considered in the ionic conductance relations in the Hodgkin-Huxley equation to simulate the action potential accurately, and it is valid for the frequencies below 5 kHz. Therefore, we discuss dispersive conductance and capacitance.

To discuss dispersion in cable theory, we propose the dispersive model of Equation (1) below since it is general, and the dispersive model of Equation (2) can be written accordingly by eliminating the ionic conductance. To express dispersive Hodgkin equation for the nodes of Ranvier, we rewrite Equation (1) in a general form as Equation (5). The capacitance dispersion of neuronal membrane as Figure 1 can be fitted by the combination of Debye and Lorentz models. The conductance dispersion of intra and extracellular media and passive membrane can be fitted by Lorentz model.

$$r_0/2\frac{\partial J_m}{\partial x} - \frac{\partial D_m}{\partial t} - \sum g_{(V_m)k}(V_m - V_{I-ch.k}) = 0 \tag{5}$$

$\hat{J}_m$ and $\hat{D}_m$ are dispersive as Lorentz and Debye models for membrane characteristics. In the first order implementation, Equations (6) and (7) show how $\hat{J}_m$ and $\hat{D}_m$ are proportional to $\hat{V}_m$ in the frequency domain.

$$\hat{D}_m = C(\omega)\hat{V}_m = \left(C_\infty + \frac{\Delta C}{1 + j\omega\tau_p} + \frac{j\omega\Delta C_a}{1 + j\omega\tau_a - \omega^2/\omega_a^2}\right)\hat{V}_m = C_\infty\hat{V}_m + \hat{D}_{m1} + \hat{D}_{ma} \tag{6}$$

$$\hat{J}_m = \sigma_m(\omega)\frac{\partial\hat{V}_m}{\partial x} = \left(\frac{1}{\rho_\infty} + \frac{j\omega\Delta\sigma_m}{1 + j\omega 2\delta - \omega^2/\omega_0^2}\right)\frac{\partial\hat{V}_m}{\partial x} = \frac{1}{\rho_\infty}\frac{\partial\hat{V}_m}{\partial x} + \hat{J}_{m1} \tag{7}$$

σ_m and $C(\omega)$ are the total dispersive conductivity and capacity functions which are expanded in relative terms in (6) and (7). These equations are in the frequency domain. However, we need to analyze the model in time domain to study the effects of excitation. By inserting Equations (6) and (7) in

Equation (4) and rewriting it in the time domain, Equation (8) is obtained.

$$r_0/2\rho_\infty \frac{\partial^2 V_m}{\partial x^2} + r_0/2 \frac{\partial J_{m1}}{\partial x} - \frac{\partial D_{m1}}{\partial t} - \frac{\partial D_{ma}}{\partial t} - C_\infty \frac{\partial V_m}{\partial t} - \sum g_{(V_m)k}(V_m - V_{I-ch.k}) = 0 \tag{8}$$

where J_{m1}, D_{ma} and D_{m1} are derived by Equations (9) and (10).

$$D_{m1} + \tau_p \frac{\partial D_{m1}}{\partial t} = \Delta C V_m \tag{9}$$

$$D_{ma} + \tau_a \frac{\partial D_{ma}}{\partial t} + \frac{1}{\omega_a^2} \frac{\partial^2 D_{ma}}{\partial t^2} = \Delta C_a \frac{\partial V_m}{\partial t} \tag{10}$$

$$J_{m1} + 2\delta \frac{\partial J_{m1}}{\partial t} + \frac{1}{\omega_0^2} \frac{\partial^2 J_{m1}}{\partial t^2} = \Delta \sigma_m \frac{\partial^2 V_m}{\partial t \partial x} \tag{11}$$

These three differential equations must be solved at each time step. J_{m1}, D_{ma} and D_{m1} of the last time step are used in Equation (8) to find V_m. Then, J_{m1}, D_{ma} and D_{m1} are obtained for the next time step using the obtained V_m.

τ_p, δ, ΔC, ω_0, ω_a, C_∞, ρ_∞ and $\Delta\sigma_m$ are constant values and specify the dispersion diagram. The accurate values are calculated by measuring. We find the parameters by fitting the relations to the measured diagrams in this article.

The achieved results for motor neuron in the thoracic region of the spinal cord are illustrated in the next section. To study the proposed method, a coil as in Figures 4 is considered as the stimulator, and results of the simulations by both dispersive and nondispersive models are compared. As presented in Roth and Basser's method, the induced electrical field (E field) by the coil is entered into the equation in the nondispersive model as follows [10]:

$$r_0/2\rho \frac{\partial^2 V_m}{\partial x^2} - r_0/2\rho \frac{\partial E_x}{\partial x} - C \frac{\partial V_m}{\partial t} - \sum g_{(V_m)k}(V_m - V_{I-ch.k}) = 0 \tag{12}$$

where E_X is a longitudinal component of E field. According to the above discussion, Equation (12) is rewritten in the dispersive model as Equation (13) to study the effect of dispersion on the nerve fiber excitability by the external stimulation.

$$\begin{aligned} &r_0/2\rho_\infty \frac{\partial^2 V_m}{\partial x^2} + r_0/2 \frac{\partial J_{m1}}{\partial x} - r_0/2\rho_\infty \frac{\partial E_x}{\partial x} - r_0/2 \frac{\partial J_E}{\partial x} - \frac{\partial D_{m1}}{\partial t} - \frac{\partial D_{ma}}{\partial t} \\ &-C_\infty \frac{\partial V_m}{\partial t} - \sum g_{(V_m)k}(V_m - V_{I-ch.k}) = 0 \end{aligned} \tag{13}$$

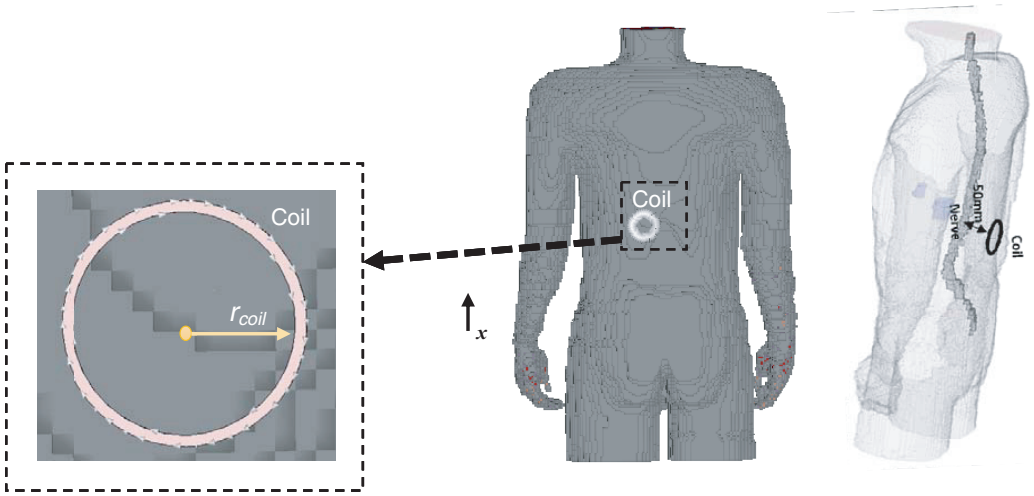

Figure 4. The Gustav human voxel is shown. Dispersive electromagnetic properties are considered for all the tissues [17] and the surrounding media is air. The coil is located on the thoracic region of a human voxel (outside the body). Distance of the coil and motor neuron is 50 mm.

where J_{m1}, D_{ma} and D_{m1} are derived by Equations (9), (10) and (11), respectively, and J_E is derived by Equation (14).

$$J_E + 2\delta\frac{\partial J_E}{\partial t} + \frac{1}{\omega_0^2}\frac{\partial^2 J_E}{\partial t^2} = \Delta\sigma_m\frac{\partial E_x}{\partial t} \tag{14}$$

Equations (9), (10), (11), (13) and (14) should be solved simultaneously. These equations are solved by the backward method for partial differential equations (PDE) as Equations (15), (16), (17), (18) and (19).

$$\begin{aligned} &r_0/2\rho_\infty\frac{\left(V^{n+1}_{m(i-1)} - 2V^{n+1}_{m(i)} - V^{n+1}_{m(i+1)}\right)}{\Delta x^2} + \frac{\left(J^{n+1}_{m1(i+1)} - J^{n+1}_{m1(i-1)}\right)}{2\Delta x} - r_0/2\rho_\infty\frac{\left(E^n_{x(i+1)} - E^n_{x(i-1)}\right)}{2\Delta x} \\ &-r_0/2\frac{\left(J^{n+1}_{E(i+1)} - J^{n+1}_{E(i-1)}\right)}{2\Delta x} - C\frac{D^{n+1}_{m1(i)} - D_{m1^n_{(i)}}}{\Delta t} - C_\infty\frac{V^{n+1}_{m(i)} - V^n_{m(i)}}{\Delta t} - \sum_k^{g^k_{(V_m)i}(V^{n+1}_{m(i)} - V^k_{I-ch.(i)})} = 0 \end{aligned} \tag{15}$$

$$D^n_{m1(i)} + \tau_p C\frac{D^{n+1}_{m1(i)} - D^n_{m1(i)}}{\Delta t} = \Delta C V^{n+1}_m \tag{16}$$

$$D^n_{ma(i)} + \tau_a\frac{D^{n+1}_{ma(i)} - D^n_{ma(i)}}{\Delta t} + \frac{1}{\omega_a^2}\frac{D^{n+1}_{ma(i)} - 2D^n_{ma(i)} + D^{n-1}_{ma(i)}}{\Delta t^2} = \Delta C_a V^{n+1}_m \tag{17}$$

$$\begin{aligned} &J_{m1} + 2\delta\frac{J^{n+1}_{m1(i)} - J^n_{m1(i)}}{\Delta t} + \frac{1}{\omega_0^2}\frac{J^{n+1}_{m1(i)} - 2J^n_{m1(i)} + J^{n-1}_{m1(i)}}{\Delta t^2} \\ &= \Delta\sigma_m\frac{\left(V^{n+1}_{m(i)} - V^{n+1}_{m(i-1)}\right)/\Delta x - \left(V^n_{m(i)} - V^n_{m(i-1)}\right)/\Delta x}{\Delta t} \end{aligned} \tag{18}$$

$$J_E + 2\delta\frac{J^{n+1}_{E(i)} - J^n_{E(i)}}{\Delta t} + \frac{1}{\omega_0^2}\frac{J^{n+1}_{E(i)} - 2J^n_{E(i)} + J^{n-1}_{E(i)}}{\Delta t^2} = \Delta\sigma_m\frac{E^{n+1}_{x(i)} - E^n_{x(i)}}{\Delta t} \tag{19}$$

where Δx is the length of the segments.

A motor neuron from thoracic region (T9–T12) of the spinal cord is selected for investigation of the frequency dispersion impact on neuronal behavior. The motor neuron is responsible for contraction of abdominal muscles. An electromagnetic circular coil is chosen to stimulate the fiber, and the coil is located and analyzed on Gustav human voxel in CST software. The coil parameters are shown in Table 1. CST software is used to extract the incident E fields computationally. It is located in the vicinity of the spinal cord, and parameter i is the current source. The coil is considered with alternating current source, and a variety of frequencies and the generated E field are computed. The distance of the coil and axon fiber is 50 mm. The geometry of the coil in the vicinity of the body is illustrated in Figure 4. Dispersive and isotropic properties are used in the simulations for all tissues based on Eleiwa's work [17].

To determine the mammalian neural cell characteristics, dispersive relation in Equations (6) and (7) are fitted to the measured capacitance and conductance diagram versus frequency. Properties of the fibers are demonstrated in Table 2, and the fitted parameters are written in Table 3. The axon is discrete in two types of segments: myelinated and nonmyelinated. Length of the node of Ranvier is assumed 1 µm, and length of myelinated sections is 1.5 mm [34]. The conductivity coefficients of the ion

Table 1. Parameters of the coil in Figure 4.

Parameter	Description	Unit	Value
i	Current	kA	3.5
r_c	Internal radius of coil	cm	2.5
N	Number of wire turns	-	1000

channels for the nodes of Ranvier, which are discussed above, are as follows [31, 32].

$$g^n_{V_mNa-fast} = g_{Na-fast}m^3h, \quad g^n_{V_mK} = g_Kn, \quad g^n_{V_mL} = g_L, \quad g^n_{V_mNa-persistant} = g_{Na-persistant}p^3 \tag{20}$$

$$\frac{\partial m}{\partial t} = \alpha_m(1-m) - \beta_m, \quad \frac{\partial n}{\partial t} = \alpha_n(1-n) - \beta_n, \quad \frac{\partial h}{\partial t} = \alpha_h(1-h) - \beta_h, \quad \frac{\partial p}{\partial t} = \alpha_h(1-h) - \beta p \tag{21}$$

$$\begin{array}{llll} \alpha_m = \dfrac{-6.57(V+10.4)}{\exp(\frac{-10.4-V}{10.3})-1} & \alpha_h = \dfrac{0.34(V+104)}{\exp(\frac{104+V}{11})-1} & \alpha_n = \dfrac{0.3}{\exp(\frac{-43-V}{5})+1} & \alpha_p = \dfrac{-0.0353(V+17)}{\exp\left(\frac{-17-V}{10.2}\right)-1} \\ \beta_m = \dfrac{0.304(V+15.7)}{\exp(\frac{15.7+V}{9.16})-1} & \beta_h = \dfrac{12.6}{\exp(\frac{-21.8-V}{13.4})+1} & \beta_n = \dfrac{0.03}{\exp(-80-V)+1} & \beta_p = \dfrac{0.000883(V+24)}{\exp\left(\frac{24+V}{10}\right)-1} \end{array} \tag{22}$$

Considering the mentioned parameters, respective code is written in Matlab software to simulate the activity of the 30 cm axon fiber by the dispersive model. The length of the axon is divided into 500 segments, and the time step is assumed 0.0001 ms for the finite different solution.

Table 2. Parameters of the nondispersive axon fiber [31, 32].

Parameter	Description	Unit	Value
r_o	Radius of axon	μm	10
V_{Na}	Sodium Nernst potential	mV	50
V_k	Potassium Nernst potential	mV	−90
V_L	Leakage Nernst potential	mV	−90
V_{rest}	Rest potential	mV	−78.5
ρ_0	Intracellular resistance per unit	Ohm.cm	70
$C_{membrane}$	Membrane's capacitance per unit area	μF/cm^2	2
C_{myelin}	Myelin capacitance	μF/cm^2	0.1
$g_{Na-fast}$	Maximum fast Na conductance	S/cm^2	3
g_K	Maximum slow K conductance	S/cm^2	0.08
$g_{Na-persis\tan t}$	Maximum persistent Na conductance	S/cm^2	0.01
g_L	Nodal leakage conductance	S/cm^2	0.007
g_{Myelin}	Myelin conductance	S/cm^2	0.001
$g_{Membrane}$	Membrane conductance	S/cm^2	0.0001

Results are compared and shown in the next section.

3. APPLICATION AND ANALYSIS/DISCUSSION

In this section, many examples are shown to illustrate when the results differ due to dispersion effect. Predicting threshold of the excitability of a neuron and noise analysis of a neuron record are discussed in the following to show the difference. The insufficient accuracy of the conventional models shows the necessity of considering dispersion. Different cases are discussed below.

To show the validity of the dispersive model for action potential propagation, a propagation of an action potential (AP), excited by voltage clamp, is considered for both dispersive and nondispersive models and compared in Figure 5. Since the nondispersive model predicts the action potential of cells similar to the experiments, it can validate our dispersive model around the frequency bandwidth of the action potential. More investigation should be achieved by stimulation with higher frequency by experiment in the lab. Figure 5 illustrates similar results for the propagation of an AP as expected, but a slight difference is observed in the rising and falling. The gradient is high at these points, and high gradient is similar to high frequency behavior. The effective capacitance is less at the higher frequencies of the dispersive model. Thus, the high gradient variations are expected to be quicker in the dispersive mode; this matter results in a slightly sharper AP signal as shown in Figure 5.

Table 3. Retrieved dispersive parameters of the axon fiber from dispersion diagrams in the literature.

Parameter	Description	Unit	Value
ρ_∞	Intracellular high resistance per unit	$\Omega \cdot$ cm	0.1929
$C_{\infty membrane}$	Membrane high capacitance	μF/cm^2	0.3
$C_{\infty myelin}$	Myelin high capacitance	μF/cm^2	0.0119
τ_p	Capacitance dispersive constant	s	50.2
τ_a	Capacitance dispersive constant	s	0.0014
$\Delta C_{membrane}$	Capacitance dispersive constant	μF/cm^2	113.66
ΔC_{myelin}	Capacitance dispersive constant	μF/cm^2	5.183
$\Delta C_{a\text{-}membrane}$	Capacitance dispersive constant	μF/cm^2	0.0023
δ	Conductance dispersive constant	s	0.0387
$\Delta\sigma_m$	Conductance dispersive constant	S/cm	1.2855
ω_0	Conductance dispersive constant	1/s	3756.3
ω_a	Conductance dispersive constant	1/s	9427

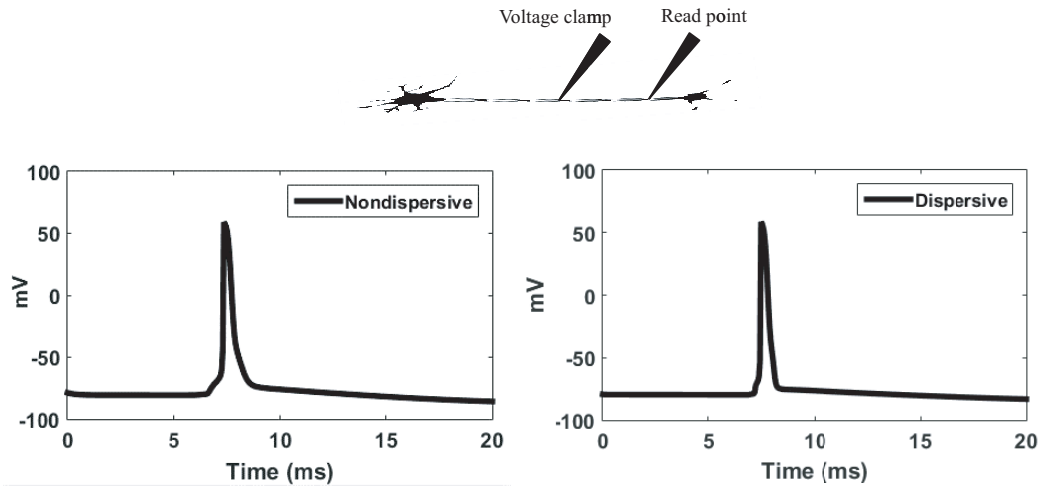

Figure 5. A motor axon fiber with 10 µm radius is selected. Dispersive and nondispersive model with characteristics in Tables 2 and 3 are considered. Comparison of action potential at one node of Ranvier by dispersive and nondispersive models is shown. Simulations show a proper similarity; as expected, the action potential is triggered by voltage clamp.

After full wave simulation of the mentioned structure, the generated E fields by the coil are shown at 1 kHz in Figure 6(a). The longitudinal component of the E field in a neuron fiber in the spinal cord is calculated and shown versus the length of the axon at 1 kHz in Figure 6(b).

Considering the mentioned E field in Figure 6, the behavior of the motor neuron fiber versus time and length of the fiber is illustrated in Figure 7. It causes maximum 1100 v/m E field in the vicinity of the axon, which is imported in Equations (13) and (14) as E_x. The simulation shows that the action potential is triggered by the mentioned electric field and propagated in the cell fiber. In the excitation form, we have both inhibitory and excitatory behaviors since the neuron is excited at threshold level in this figure and is due to the spatial E-field form. The excitation and inhibition regions change over time. Therefore, AP propagates in the direction that is located on the excitatory behavior at the starting time, and the other direction is inhibited by lower membrane potential according to the inhibitory E-field form. If the neuron is excited by higher magnitude of E field, AP is excited and propagates on both sides.

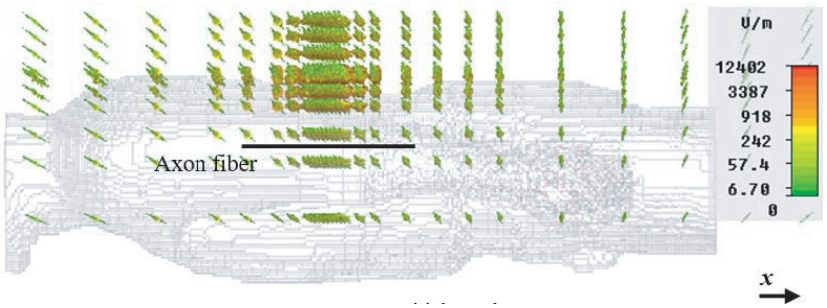

(a)

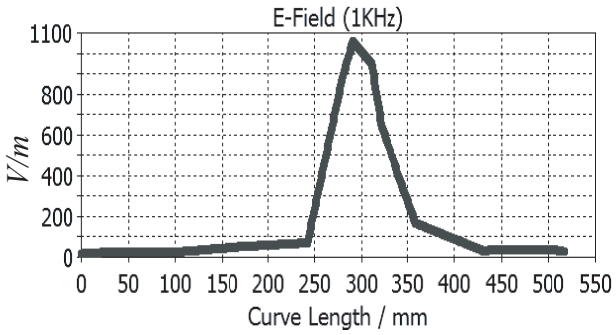

(b)

Figure 6. The electric field radiated by the coil, mentioned in Table 1 and shown in Figure 4. (a) Three dimensional view of electric fields inside and outside the body is shown. The maximum electric field is 12 kV/m outside the body, but the maximum value of the electric field inside the body is 1.2 kV/m. (b) The longitudinal component of the electric field in the mentioned fiber is plotted versus the length of the motor neuron fiber.

Afterwards, the generated E-field form by the coil is extracted at different frequencies and inserted in Equations (13) and (14) as an external electric field (E_x) to find the electrical threshold of excitability. Thresholds are determined by finding the minimum value of longitudinal electrical field on the axon fiber that excites the action potential. The current source of the coil is in $i*\sin(\omega t)$ format, and consequently, the E fields are in the form of $Ps * A(x) * \cos(\omega t)$. $A(x)$ is the normalized function of axon length in Figure 6(b), and the threshold values refer to the maximum value of E field (Ps). The periods of the simulations are set to 10 stimulation cycle while the frequency of stimulation is lower than 50 Hz; for the frequencies more than 50 Hz, the period is set to 200 ms. These periods assure us to consider the whole transient time of neuronal activity and stationary time in the effect of the induced electric fields.

The following study is performed to show the difference between the conventional and dispersive models. In Figure 8, the required longitudinal E field to excite the cell is depicted versus the frequency of stimulation. Rate of stimulation influences the results due to the impact of the effective duration of stimulation in membrane excitability. Impact of stimulation rate is the opposite of the dispersion effect of the membrane. However, the results indicate that the impact of the stimulation rate is dominant to the dispersion effect. The figure shows that the predictions of the dispersive and conventional methods differ at low and high frequencies, which shows the necessity of using dispersive model over the conventional one. According to the nonlinear behavior of membrane, the exact analysis is hard, and differences in the results of both models are due to the combination of both anomalous inductive reactance and higher frequency impact. If the anomalous inductive reactance is neglected, the differences between the diagrams are less at the frequencies lower than 1 kHz. Slope of the changes in the diagrams by nondispersive model in Figure 8 increases by the increase in frequency although it differs in the dispersive model. At less frequencies, the threshold increases with frequency due to both an increase in the effective capacitance of the membrane and a decrease in the effective duration of excitation, but the slope of the diagram decreases, and the threshold increases slowly by increasing the frequency due to the decreasing value of the effective capacitance.

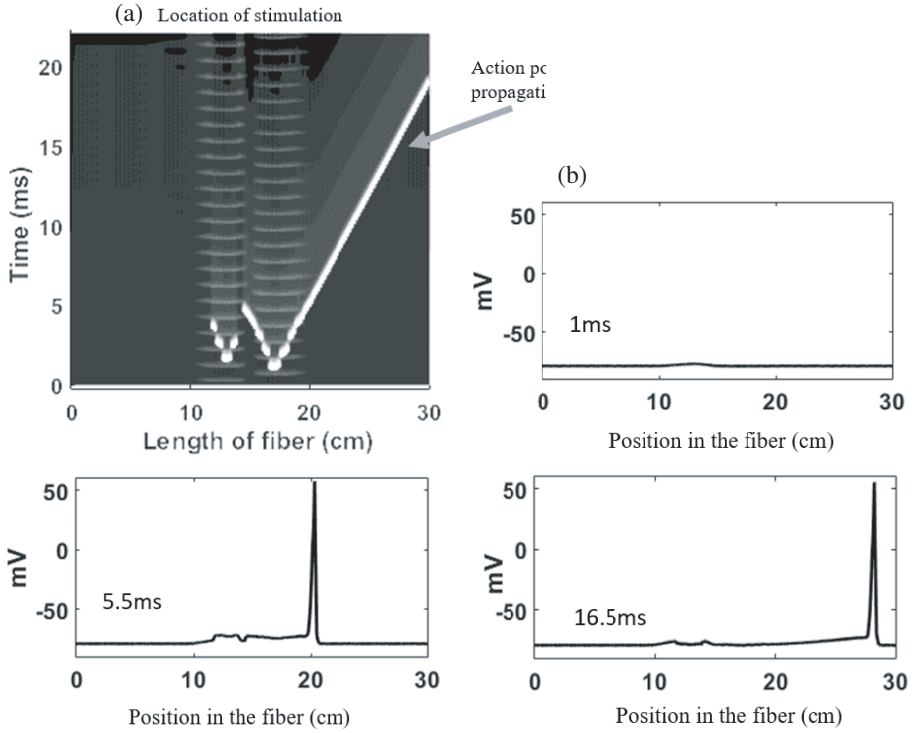

Figure 7. (a) Excitation of membrane voltages versus position in the axon fiber and time by 1 kHz and 1100 V/m sinusoidal stimulation. The duration of the simulation is 20 ms and action potential propagation is shown by the white path. (b) Membrane voltages versus the position in the fiber in 3 discrete times after the start of the stimulation.

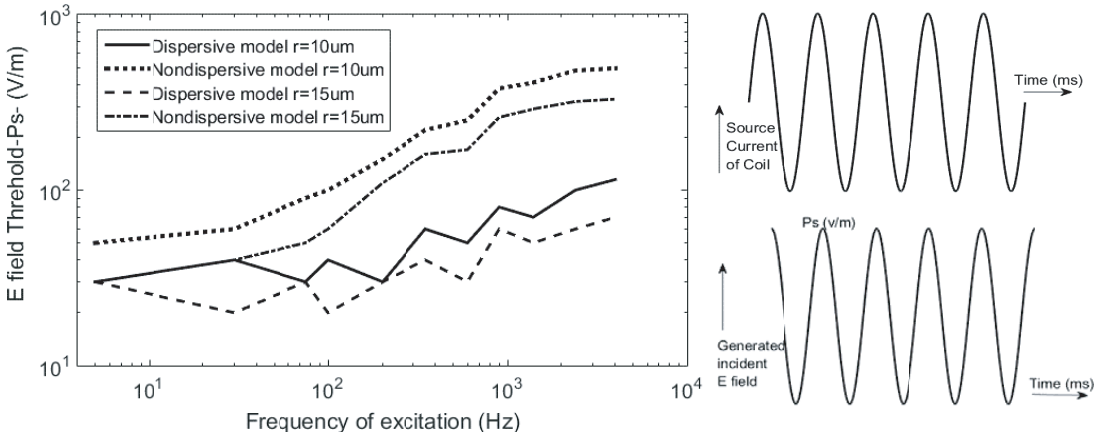

Figure 8. Sinusoidal signal form for current of stimulator coil in Figure 4 is selected. The form of incident electric field, according to stimulation signal is shown. Comparison of the predicted required longitudinal E field for excitation by conventional and dispersive models in two fibers with different radii of 10 μm and 15 μm are shown. The characteristics are mentioned in Tables 2 and 3.

Figure 8 is useful for investigating the effect of devices which produce permanent fields such as high voltage transformers. However, most excitation devices use pulses as the signal of excitation. Therefore, we discuss two pulse excitation signals below. Most works in the literature focus on the time form of excitation signal as the injection current or voltage clamp, and the investigation of nondestructive excitation is neglected. There is a difference between the effects of injected current and source current

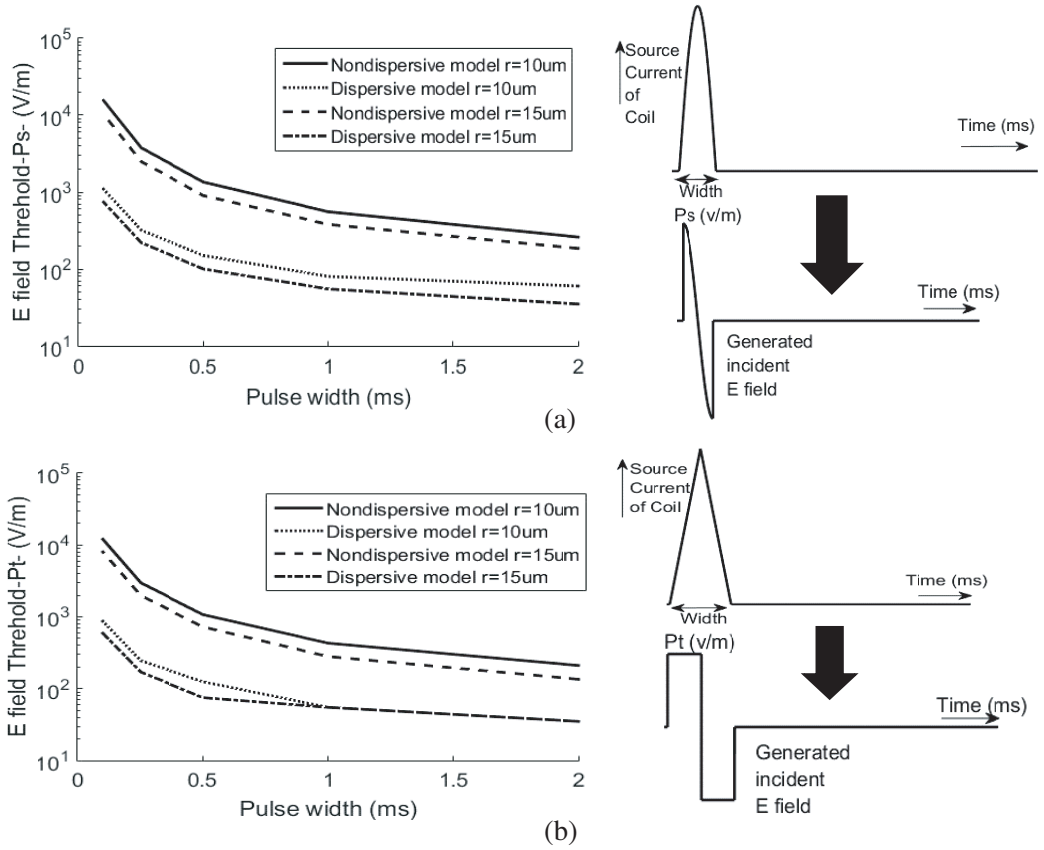

Figure 9. Two signal forms for current in stimulator coil in Figure 4 are selected. The forms of incident electrical fields according to stimulation signals are shown. Comparison of the predicted required longitudinal E field for exciting neurons is shown by conventional and dispersive models. Two motor neuron fibers are selected. Radii of neurons are 10 µm and 15 µm and the characteristics are mentioned in Tables 2 and 3.

of a coil or other radiators. The derivative of the current signal of the coil in time results in the time form of the radiated E field. Therefore, the shape of the effective excitation signal differs from the source signal in time. Only the impact of signal form in direct injection or potential based excitation is discussed in the literature. Here, we consider this point by investigating two pulses as the source of the mentioned coil. Responses of the nerve fiber to two different current signals as the source current of the coil versus the variety of pulse widths are illustrated in Figure 9. The estimated required E field for excitation is shown by both dispersive and nondispersive models. Pulses are narrow in time; the Fourier transforms of the signal are wide in the frequency domain; the peaks of the diagram are mostly at higher frequencies, which requires dispersive analysis. Therefore, the estimated thresholds by conventional models differ noticeably from that by dispersive model.

The difference between predicted thresholds in Figure 9 illustrates the use of dispersive modeling in the pulse analysis. Figure 9 shows that the required E field is increased by increasing excitation frequency. On the other hand, most radiators generate higher magnitude of E fields by increasing frequency or shortening the source pulse width. Thus, researchers consider the capabilities of radiators and, using Figures 8 and 9, can find the best frequency and pulse width for their experiments.

Another advantage of using dispersive modeling is the ability of considering the noise in the analysis. The noise signal includes a wide frequency spectrum, and the conventional models filter the high frequency changes. However, dispersive modeling can determine the effect of noise in the responses of neural fibers, which is depicted in Figure 10. The current is injected into the fiber, and the membrane potential is plotted by both conventional and dispersive modelings. Injected current signal

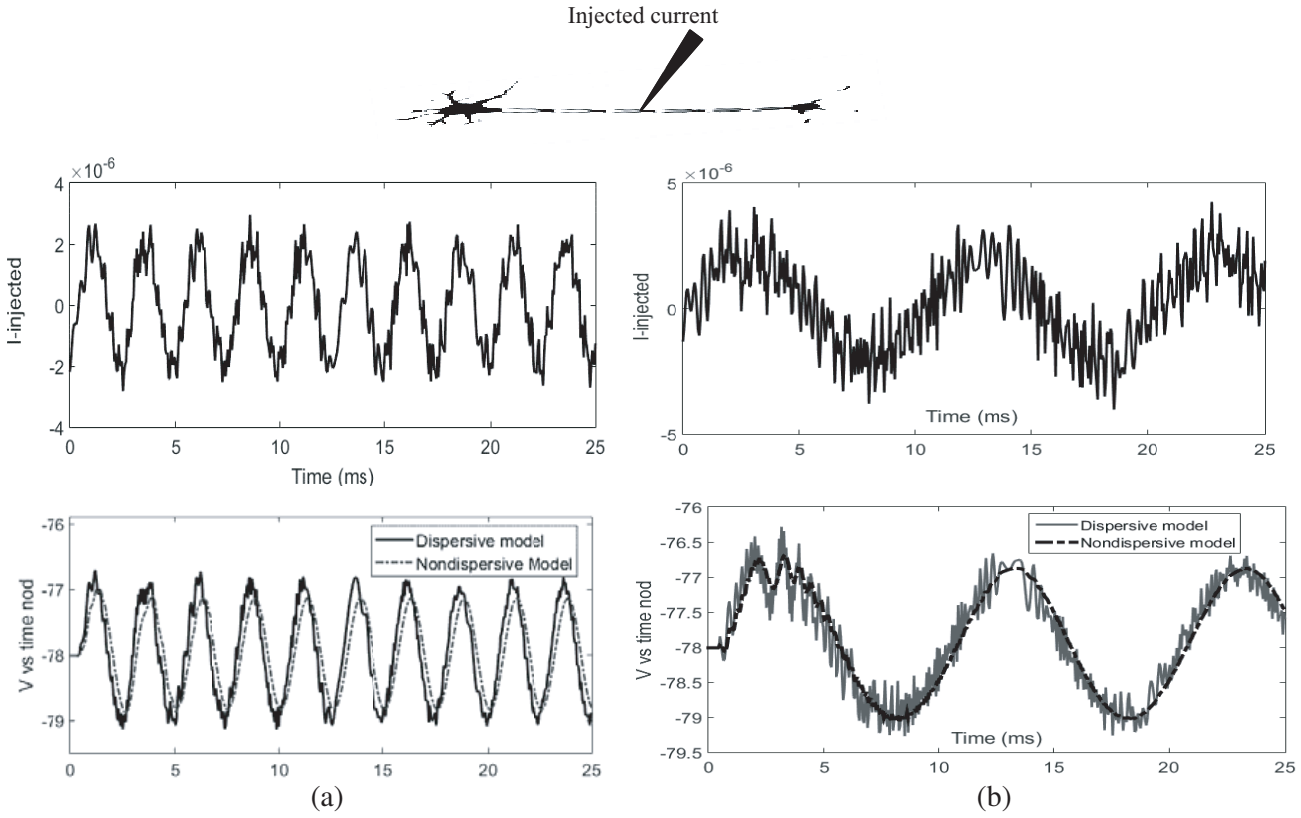

Figure 10. Membrane potential changes after the injection of noisy current into the fiber by dispersive and nondispersive models. Required characteristics of the models are mentioned in Tables 2 and 3. (a) 400 Hz noisy stimulation, (b) 40 Hz noisy stimulation. Noisy injected current and consequently membrane potential variation are shown.

is the sum of a sine function of time and noise function. The corresponding membrane response is also shown. Noise effect is not demonstrated in the conventional model sufficiently while it is obvious in dispersive modeling. Neuronal noise explains random influences on the transmembrane voltage of single or a group of neurons. This noise can influence the transmission and integration of signals from other neurons as well as firing the activity of neural networks.

The main measure of the action of noise is seen in neuronal firing variability. Noise effects are investigated on different spatial and temporal scales in single neurons, from the molecular level all the way up to firing activity on the scale of the whole brain as seen in EEG or MEG recordings and behavioral outputs. Given the number of nonlinear processes in the nervous system and the effects that noise can have on nonlinear systems, it is not surprising that stochastic neuronal dynamic is a particularly active area of research, which shows the significance of using dispersive model in direct and reverse analyses of neurons over the conventional models.

Generally, the generated signals from many therapeutic devices are at the frequency of higher than 1 kHz or have more than 2 kHz bandwidths at low frequencies. Designing stimulator or therapeutic devices requires authentic determination of the behavior of excitable cell under radiation. More accurate simulation means more effective treatment. We proposed how to extend the Hodgkin-Huxley model to consider dispersion. The difference shows the necessity of considering dispersion. Constant conductance may be approximately authentic for AP propagation, but by inserting an external electrical field with any frequency, the potential distribution will be different for different frequencies. The potential distribution specifies the region of excitation, which can change the output. Our model considers both the anomalous inductive reactance behavior and dispersive conductance in addition to dispersive capacitance unlike previous model. Neglecting the anomalous inductive reactance behavior means uncertain results under 200 Hz and 30% error.

4. CONCLUSION

Nondestructive methods are being presented every day. Biological tissues are complex, and accurate modeling is required to analyze and design new devices. One of the complexities in electrical analysis is the dispersion of biological tissues. In this paper, a dispersive cable model of excitable cells is proposed to consider the dispersivity of the tissues. Lorentz and Debye model is used to model the dispersivity. Axon of the motor neuron is stimulated by induced electric field to study the proposed model. The estimated required E field is incremented by increasing the frequency in both dispersive and nondispersive models, although the magnitude and behavior of the threshold E field differ significantly versus frequency. Changes in both effective resistance and capacitance influence the membrane reaction to the excitation. Therefore, according to excitation, the signal frequency spectrum results may differ even more than 100% at the frequencies of higher than 3 kHz. This model results in considering various external fields and excitation as pulse or continuous forms. Signal form optimization and analysis are possible based on the model. Since many of the stimulator devices work at various frequencies and record devices cover wide band signals from neuronal activities, the proposed dispersive method can assist in accurate device design. Noise analysis is achievable by this model, unlike conventional models. Researchers are able to investigate noise effects on different spatial and temporal scales in single neurons or central nervous system, EEG and MEG records.

REFERENCES

1. Hodgkin, A. L. and A. F. Huxley, "A quantitative description of membrane current and its application to conduction and excitation in nerve," *The Journal of Physiology*, Vol. 117, No. 4, 500, 1952.
2. Gabbiani, F. and S. J. Cox, *Mathematics for Neuroscientists*, Academic Press, 2010.
3. Koch, C. and I. Segev, eds., *Methods in Neuronal Modeling: From Ions to Networks*, MIT Press, 1998.
4. Roth, B. J. and P. J. Basser, "A model of the stimulation of a nerve fiber by electromagnetic induction," *IEEE Transactions on Biomedical Engineering*, Vol. 37, No. 6, 588–597, 1990.
5. Bernardi, P. and G. D'Inzeo, "A nonlinear analysis of the effects of transient electromagnetic fields on excitable membranes," *IEEE Transactions on Microwave Theory and Techniques*, Vol. 32, No. 7, 670–679, 1984.
6. Goetz, S. M., C. N. Truong, M. G. Gerhofer, A. V. Peterchev, H.-G. Herzog, and T. Weyh, "Analysis and optimization of pulse dynamics for magnetic stimulation," *PloS One*, Vol. 8, No. 3, e55771, 2013.
7. Holt, G. R., "A critical reexamination of some assumptions and implications of cable theory in neurobiology," Ph.D. diss., California Institute of Technology, 1997.
8. Rattay, F., "Analysis of models for extracellular fiber stimulation," *IEEE Transactions on Biomedical Engineering*, Vol. 36, No. 7, 676–682, 1989.
9. Joucla, S. and B. Yvert, "Modeling extracellular electrical neural stimulation: From basic understanding to MEA-based applications," *Journal of Physiology-Paris*, Vol. 106, No. 3, 146–158, 2012.
10. Basser, P. J. and B. J. Roth, "Stimulation of a myelinated nerve axon by electromagnetic induction," *Medical and Biological Engineering and Computing*, Vol. 29, No. 3, 261–268, 1991.
11. Hirata, A., J. Hattori, I. Laakso, A. Takagi, and T. Shimada, "Computation of induced electric field for the sacral nerve activation," *Physics in Medicine and Biology*, Vol. 58, No. 21, 7745, 2013.
12. Warman, E. N., W. M. Grill, and D. Durand, "Modeling the effects of electric fields on nerve fibers: Determination of excitation thresholds," *IEEE Transactions on Biomedical Engineering*, Vol. 39, No. 12, 1244–1254, 1992.
13. Pashut, T., S. Wolfus, A. Friedman, M. Lavidor, I. Bar-Gad, Y. Yeshurun, and A. Korngreen, "Mechanisms of magnetic stimulation of central nervous system neurons," *PLoS Computational Biology*, Vol. 7, No. 3, e1002022, 2011.

14. King, R. W. P., "Nerves in a human body exposed to low-frequency electromagnetic fields," *IEEE Transactions on Biomedical Engineering*, Vol. 46, No. 12, 1426–1431, 1999.
15. Liston, A., R. Bayford, and D. Holder, "A cable theory based biophysical model of resistance change in crab peripheral nerve and human cerebral cortex during neuronal depolarisation: Implications for electrical impedance tomography of fast neural activity in the brain," *Medical & Biological Engineering & Computing*, Vol. 50, No. 5, 425–437, 2012.
16. Howell, B., L. E. Medina, and W. M. Grill, "Effects of frequency-dependent membrane capacitance on neural excitability," *Journal of Neural Engineering*, Vol. 12, No. 5, 056015, 2015.
17. Eleiwa, M. A. and A. Z. Elsherbeni, "Debye constants for biological tissues from 30 Hz to 20 GHz," *ACES Journal*, Vol. 16, No. 3, 2001.
18. Takashima, S. and H. P. Schwan, "Passive electrical properties of squid axon membrane," *The Journal of Membrane Biology*, Vol. 17, No. 1, 51–68, 1974.
19. Cole, K. S., "Electrical properties of the squid axon sheath," *Biophysical Journal*, Vol. 16, No. 2, 137–142, 1976.
20. Cole, K. S., "Rectification and inductance in the squid giant axon," *The Journal of General Physiology*, Vol. 25, No. 1, 29–51, 1941.
21. Cole, K. S. and R. F. Baker, "Longitudinal impedance of the squid giant axon," *The Journal of General Physiology*, Vol. 24, No. 6, 771–788, 1941.
22. Cole, K. S. and R. F. Baker, "Transverse impedance of the squid giant axon during current flow," *The Journal of General Physiology*, Vol. 24, No. 4, 535–549, 1941.
23. Cole, K. S. and G. Marmont, "The effect of ionic environment upon the longitudinal impedance of the squid giant axon," *Fed. Proc.*, Vol. 1, 15–16, 1942.
24. Cole, K. S., *Membranes, Ions, and Impulses: A Chapter of Classical Biophysics*, Vol. 5, Univ. of California Press, 1968.
25. Grant, P. F. and M. M. Lowery, "Effect of dispersive conductivity and permittivity in volume conductor models of deep brain stimulation," *IEEE Transactions on Biomedical Engineering*, Vol. 57, No. 10, 2386–2393, 2010.
26. Nagarajan, S. S., D. M. Durand, and E. N. Warman, "Effects of induced electric fields on finite neuronal structures: A simulation study," *IEEE Transactions on Biomedical Engineering*, Vol. 40, No. 11, 1175–1188, 1993.
27. Miranda, P. C., L. Correia, R. Salvador, and P. J. Basser, "Tissue heterogeneity as a mechanism for localized neural stimulation by applied electric fields," *Physics in Medicine and Biology*, Vol. 52, No. 18, 5603, 2007.
28. Silva, S., P. J. Basser, and P. C. Miranda, "Elucidating the mechanisms and loci of neuronal excitation by transcranial magnetic stimulation using a finite element model of a cortical sulcus," *Clinical Neurophysiology*, Vol. 119, No. 10, 2405–2413, 2008.
29. Platkiewicz, J. and R. Brette, "A threshold equation for action potential initiation," *PLoS Computational Biology*, Vol. 6, No. 7, e1000850, 2010.
30. Ying, W. and C. S. Henriquez, "Hybrid finite element method for describing the electrical response of biological cells to applied fields," *IEEE Transactions on Biomedical Engineering*, Vol. 54, No. 4, 611–620, 2007.
31. McIntyre, C. C., et al., "Modeling the excitability of mammalian nerve fibers: Influence of afterpotentials on the recovery cycle," *Journal of Neurophysiology*, Vol. 87, No. 2, 995–1006, 2002.
32. McIntyre, C. C. and W. M. Grill, "Extracellular stimulation of central neurons: Influence of stimulus waveform and frequency on neuronal output," *Journal of Neurophysiology*, Vol. 88, No. 4, 1592–1604, 2002.
33. Oughstun, K. E. and N. A. Cartwright, "On the Lorentz-Lorenz formula and the Lorentz model of dielectric dispersion," *Optics Express*, Vol. 11, No. 13, 1541–1546, 2003.
34. Kandel, E. R., J. H. Schwartz, and T. M. Jessell, (Eds.), *Principles of Neural Science*, Vol. 4, 71–171, McGraw-Hill, New York, 2000.